Enhanced and Selective MALDI-MS Detection of Peptides via the Nanomaterial-Dependent Coffee Ring Effect

Jutiporn Yukird,[a] Cameron J. Kaminsky,[b] Orawon Chailapakul,[c] Nadnudda Rodthongkum,[a,d *] and Richard W. Vachet[b*]

[a]Metallurgy and Materials Science Research Institute, Chulalongkorn University, Phayathai Road, Patumwan, Bangkok 10330, Thailand

[b]Department of Chemistry, University of Massachusetts Amherst, Amherst, Massachusetts 01003, United States

[c]Electrochemistry and Optical Spectroscopy Center of Excellence, Department of Chemistry, Faculty of Science, Chulalongkorn University, Phayathai Road, Patumwan, Bangkok 10330, Thailand

[d]Center of Excellence in Responsive Wearable Materials, Chulalongkorn University, Bangkok 10330, Thailand

*Corresponding author email addresses: rwvachet@chem.umass.edu; Nadnudda.R@chula.ac.th

Abstract

Nanomaterials have been explored as alternative matrices in MALDI-MS to overcome some of the limitations of conventional matrices. Recently, we demonstrated a new means by which nanomaterials can improve peptide ionization and detection in MALDI-MS analyses by exploiting the tendency of nanomaterials to form 'coffee rings' upon drying from liquids. In the current work, we investigate how nanomaterial size and composition affect the signal enhancement of peptides through the coffee-ring effect. From studies of eight different types of nanomaterials ranging in size and composition, we find that most nanomaterials can provide signal enhancement ranging from 2- to 10-fold for individual peptides, as long as a coffee ring is formed. However, when a mixture of peptides is present in a sample, the signal enhancement is the greatest for peptides whose net charge is complementary to the nanomaterial's surface charge. These results suggest that careful design of NM surface properties could allow for selective, enhanced MALDI-MS detection of specific peptides in complex mixtures.

Keywords: Coffee ring effect, MALDI-MS, particle-peptide binding efficiency, signal enhancement, nanomaterials

Introduction

Matrix-assisted desorption ionization mass spectrometry (MALDI-MS) is a soft ionization technique that has been widely used to detect various molecules because of its high sensitivity, high throughput, minimal sample consumption, and ability to be used in an imaging context. Various matrices have been used for MALDI-MS to facilitate ionization. Conventional organic matrices consisting of extended π-conjugated systems and polar acidic or basic functional groups are commonly used.[1-9] However, conventional organic matrices have some limitations, such as low m/z interferences and spot-to-spot signal variability that have inspired the search for new matrices.[10-13]

Nanomaterials (NMs) have been studied extensively as alternate matrices because (i) they typically do not have low m/z interferences and/or (ii) they can be used to simultaneously enrich analytes for more selective detection.[14-16] NMs often have unique optical properties, energy transfer characteristics, high surface areas, and high conductivities that make them very useful materials in MALDI-MS.[17,18] Surface-functionalized NMs can enable selective analyte capture while also acting as matrices that facilitate analyte ionization and detection.[15,19,20] Carbon-based NMs,[21,22] metal-core NMs,[18,23-27] and metal oxide-based NMs[28-31] have been most commonly applied to assist desorption/ionization of analytes, and some of these materials can also be used to selectively trap target molecules via electrostatic interactions, covalent binding, or hydrophobic interactions.

Much less attention has been paid to how NM-based matrices could improve spot-to-spot signal variability. The formation of analyte "sweet spots" when using conventional organic matrices is a common problem that arises from inhomogeneous distributions of analyte-matrix crystals, which can negatively influence quantitative analyses in MALDI-MS.[32,33] Some work has

shown that careful spotting procedures,[34] layer-by-layer NM deposition, [35,36] and the proper choice of size and preparation conditions[37, 38] can improve sample homogeneity when using NM matrices, but none of these studies has used the inherent properties of NM to improve spot-to-spot signal variability. We recently demonstrated that the tendency of nanoparticle-containing liquids to form a 'coffee ring' upon drying can be used to improve sample homogeneity and enhance analyte detection.[39] In that proof-of-concept work, we demonstrated that the coffee ring effect helps concentrate analytes into a smaller area, overcoming spot-to-spot heterogeneity while also reducing low m/z interferences. The coffee-ring effect itself has been extensively studied, providing useful insight that could be used to further enhance the MALDI-MS detection of biomolecules in the presence of NMs. Factors such as evaporation rate, particle size, particle composition, and solution composition[40-42] affect coffee-ring formation, and are variables that should be investigated to further improve signal enhancement.

Here, we describe how NM composition affects MALDI-MS signal enhancement for individual peptides and peptide mixtures through the coffee ring effect. We find that NM composition has a relatively minor effect on signal enhancement as long as a robust coffee ring is formed. Peptide identity has a more notable effect on signal enhancement, especially in peptide mixtures where the enhancement is greatest for peptides and NMs having opposite charges. Our results suggest that peptides in a mixture compete for binding sites on the NMs, allowing some selectivity in peptide detection. Overall, the results presented here demonstrate that a wide array of NMs can be used to enhance peptide signal in MALDI, and careful design of NM surface properties and coffee ring formation conditions could allow for more selective peptide detection.

Materials and methods

Chemicals and materials

α-cyano-4-hydroxycinnamic acid (CHCA) was purchased from Sigma-Aldrich (St. Louis, MO). The peptides angiotensin I (MW 1296, DRVYIHPFHL), angiotensin II (MW 1046, DRVYIHPF), ANP (MW 1225, SLRRSSCFGGR), bradykinin (MW 1060, RPPGFSPFR), β-amyloid (10-20), kinetensin (MW 1172, IARRHPYFL), and preproenkephalin (MW 1955, SSEVAGEGDGDSMGHEDLY) were purchased from the American Peptide Company (Sunnyvale, CA). Bovine serum albumin (BSA) digest was purchased from New England Biolabs (MA, USA). Citrate gold nanoparticles (AuNPs) with 20 nm core sizes (Product#: 741965) and graphene quantum dot (GQD) with 5 nm core sizes (Product#: 900712) were purchased from Sigma-Aldrich (St. Louis, MO). TEGOH AuNPs, which have an alkanethiolate surface coating that is terminated by tetraethylene glycol groups (Scheme S1), were synthesized using published methods.[18,39] Details of the synthesis are included in the SI. Graphene oxide (GO) was purchased from Graphene Supermarket (New York, USA). MXenes, including ones doped with the metals Co, Fe, and Ni, were prepared using previously described methods,[43] and details of the syntheses are included in the SI. Deionized water was obtained from a Millipore Simplicity 185 Milli-Q system. All other chemicals were used as their purchased forms.

Characterization of the NMs

The zeta-potential of nanomaterials was determined using a Zetasizer Nano-ZS (Malvern Instruments, UK). All nanomaterials were dispersed in deionized distilled water for analysis. The analysis was performed at 25 °C using a scattering angle of 173°. All data are derived from at least three independent experiments.

Sample preparation

The NMs were dissolved in deionized water at the desired concentration and sonicated for 15 min. The MALDI matrix CHCA was prepared as a stock solution at 30 mg/mL and diluted to the desired concentrations with a mixture of acetonitrile:water (70:30). To achieve complete dissolution of the CHCA solution at 30 mg/mL, the solution was sonicated and heated for 30 min. The peptides were dissolved in water and were mixed with the NM solution at the concentrations of interest. Then, 5 μL of the NM/peptide sample was further mixed with 5 μL of matrix solution to achieve the desired concentrations, with the acetonitrile:water ratio 35:65. A 1 μL aliquot of the NM/peptide/matrix mixture was then directly deposited onto a stainless steel target and allowed to dry at room temperature. After solvent evaporation and sample crystallization, the target plate was introduced into mass spectrometer for MALDI-MS analysis.

MALDI-MS analysis

All MS analyses were performed on a Bruker Autoflex III MALDI-TOF mass spectrometer that is equipped with a Nd:YAG laser (355 nm) that is part of the Smartbeam system. To acquire a single mass spectrum, 250 laser shots were fired at a frequency of 100 Hz at 30% of the full laser power. These laser shots were spread across at least 10 random locations on the sample spot. For studies of the coffee ring, these 10 different locations were chosen to be in the visible ring as observed by the Autoflex's camera. For analyses in the interior of coffee-ring forming spots, these 10 different locations were chosen to be far from the visible coffee ring. Most MALDI experiments were conducted with a laser spot size of 0.15 mm, whereas the MS imaging experiments were done on some samples using a laser-beam raster width of 25 μm. After the MALDI-MS imaging experiments, the m/z values of interest were selected to generate images of the analyte distributions.

RESULTS AND DISCUSSION

NM type affects coffee ring formation and MALDI signal enhancement

NMs of various sizes and compositions (Table S1) were investigated for their ability to enhance peptide detection during MALDI-MS analysis. In our previous work,[39] we found that low CHCA matrix concentrations (≤ 2.5 mg/mL) were important to facilitate coffee ring formation and ion signal enhancement. For the NMs studied here, we find that similarly low matrix concentrations are necessary, with matrix concentrations between 0.25 and 0.5 mg/mL being optimal for most NMs. It should be noted that these matrix concentrations are much lower than CHCA concentrations (~15 mg/mL) that are used in conventional MALDI-MS analysis, and no coffee ring is formed without NMs present. A wide range of NM concentrations (0.005 – 0.35 mg/mL) are suitable for forming coffee rings and providing signal enhancement, although the thickness of the coffee ring is affected by NM concentration, as has been shown previously.[41] Some NMs formed less well-defined coffee rings than others, and this is consistent with the known effect of NM size,[41,44] with smaller NMs forming more discrete coffee rings (Figure S1). As an example, citrate AuNPs, which are 17 nm in diameter, form a more well-defined ring than the MXene NMs, which have sizes closer to 1000 nm (Figure 1a – c). As has been observed in previous work,[45] it is likely that the larger NMs flocculate in the interior of the droplet during evaporation, preventing a more homogenous coffee-ring from forming. This variation in ability to form coffee rings directly influences the distribution of matrix and peptide signals on the target surface. The smaller NMs, like the citrate AuNPs, generate ion signals predominantly in the ring, while the larger NMs, like the MXenes, yield more heterogeneously distributed ion signals (Figure 1d and e). It should be noted that low matrix concentrations (i.e. 0.25 – 0.5 mg/mL) without the NMs or the NMs alone without matrix provide no ion signal for peptides at 1 pmol levels (Figure S2).

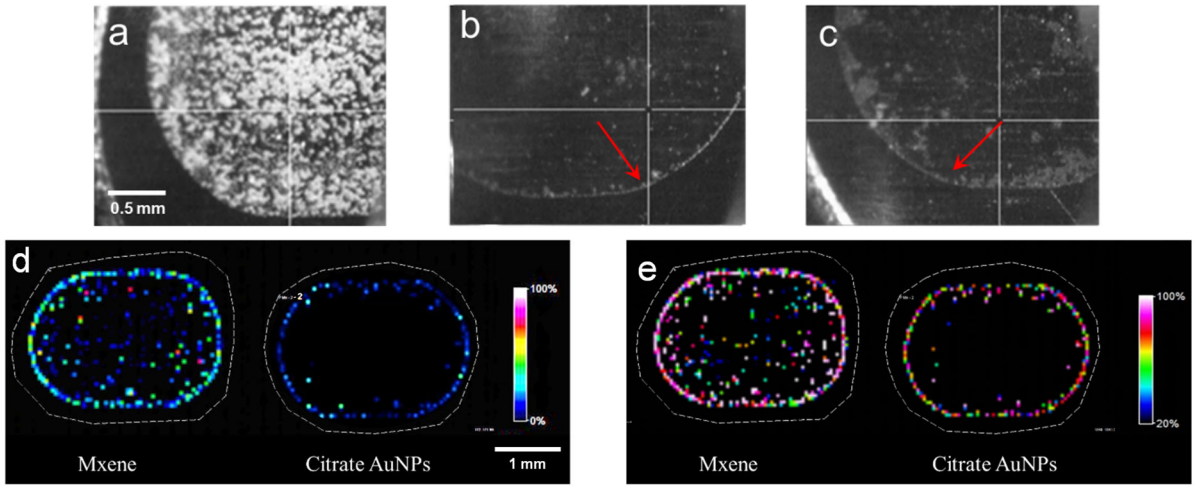

Figure 1: Optical and MS images of samples prepared for conventional MALDI-MS and coffee-ring enhanced MALDI-MS. (a) Optical image from 1 µL of a conventional matrix (15 mg/mL CHCA) preparation with the peptide bradykinin at 1 µM. (b) Optical image of the coffee ring formed from a 1 µL solution of 0.25 mg/mL of citrate AuNPs, 0.25 mg/mL CHCA matrix, and 1 µM bradykinin. (c) Optical image of the coffee ring formed from a 1 µL solution of 0.25 mg/mL of MXene, 0.25 mg/mL CHCA matrix, and 1 µM bradykinin. (d) MALDI-MS images of the CHCA matrix signal (m/z 172) from a coffee ring formed from a 1 µL solution of 0.25 mg/mL of MXene or citrate AuNPs, 0.25 mg/mL CHCA matrix, and 1 µM bradykinin. (e) MALDI-MS images of the bradykinin signal (m/z 1060) from a coffee ring formed from a 1 µL solution of 0.25 mg/mL of MXene or citrate AuNPs, 0.25 mg/mL CHCA matrix, and 1 µM bradykinin.

Despite NM differences in coffee ring formation, signal enhancements relative to conventional MALDI are observed for all the tested NMs except GO. Figure 2 shows representative mass spectra of the peptide bradykinin analyzed by conventional MALDI as compared to bradykinin analyzed with various coffee-ring forming NMs. In all cases, except for GO, the protonated bradykinin signal is higher when NMs are used than when conventional CHCA concentrations (i.e. 15 mg/mL) are used. Generally speaking, we observe signal enhancements of between 2- and 10-fold, depending on NM identity and concentration and peptide identity. Table 1 shows a representative set of signal enhancement values for the peptide bradykinin for different NMs. The TEGOH AuNPs, citrate AuNPs, and MXene NMs doped with Co(II) or Ni(II) provide the greatest enhancement for bradykinin, and these NMs also typically yield the highest signal enhancement values for most other peptide as well (e.g. Table S2).

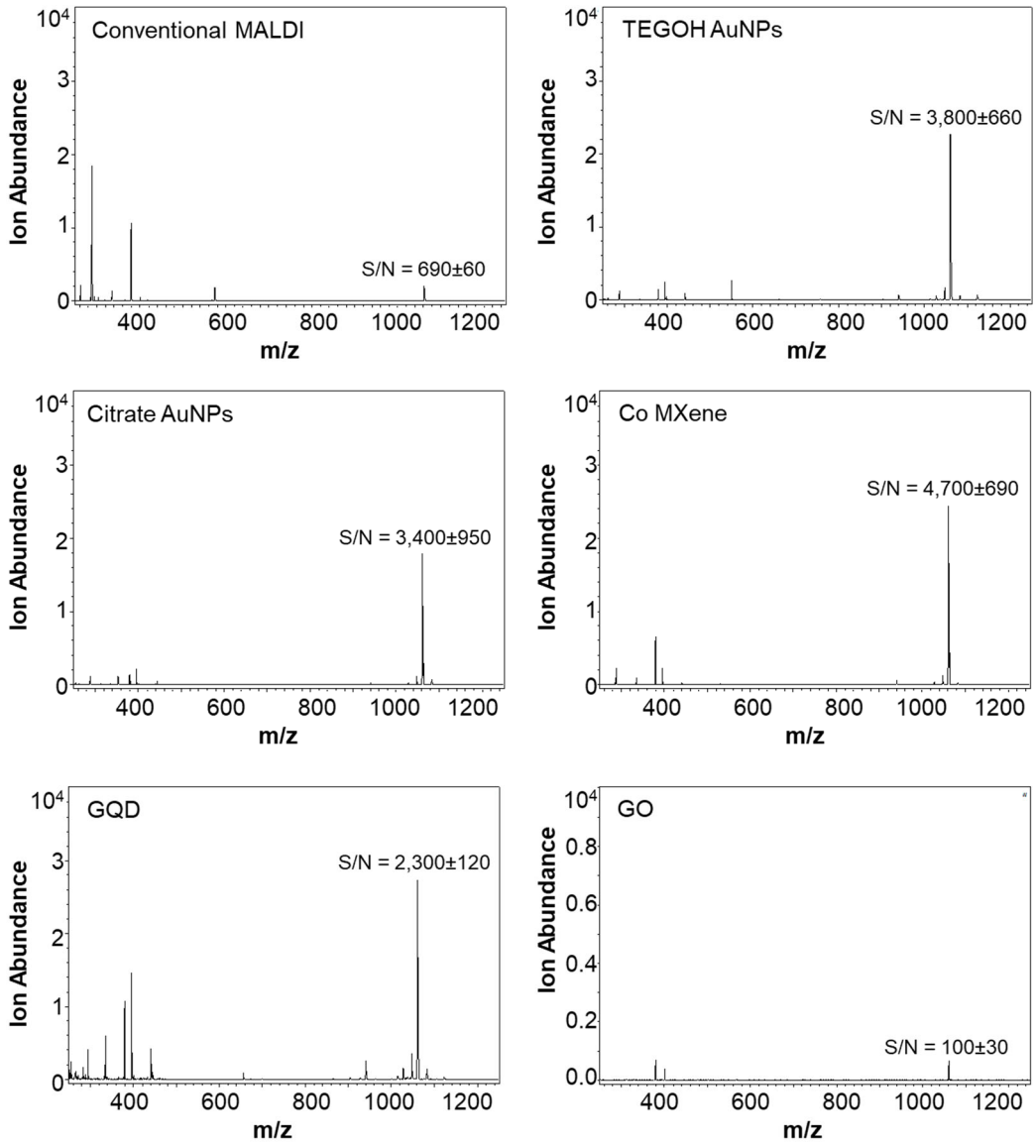

Figure 2: Representative MALDI mass spectra of 1 μM bradykinin by conventional MALDI (15 mg/mL CHCA) and from coffee-ring enhanced MALDI with different NMs, including 0.35 mg/mL TEGOH, 0.125 mg/mL citrate-AuNPs, 0.125 mg/mL Co-MXene, and 0.025 mg/mL GQD. In the NM preparations, the CHCA matrix concentration was 0.25 mg/mL.

Table 1: Ion abundances, signal-to-noise (S/N) ratios, and signal enhancement factors for the coffee-ring enhanced MALDI analysis of 1 μM bradykinin.

Matrix	NM concentration[a] (mg/mL)	Ion abundance[b]	S/N ratio[b]	Signal enhancement factor[c]
Conventional MALDI	N/A	2,200 ± 100	690 ± 60	1.0
TEGOH AuNPs	0.35	22,000 ± 4,000	3,800 ± 700	5.5
Citrate AuNPs	0.125	17,000 ± 2,000	3,000 ± 1000	5.0
Mxene	0.25	6,000 ± 1,000	1,800 ± 300	2.6
Co-Mxene	0.25	23,000 ± 5,000	4,700 ± 700	6.9
Ni-Mxene	0.25	23,000 ± 1,000	4,400 ± 200	6.5
Fe-Mxene	0.25	7,600 ± 400	2,600 ± 700	3.8
GO	0.125	400 ± 90	100 ± 30	0.2
GQD	0.025	24,000 ± 3,000	2,300 ± 120	3.3

[a] In all cases, except the conventional MALDI analysis, the CHCA concentration in the sample was 0.25 mg/mL. For conventional MALDI, the CHCA concentration was 15 mg/mL.
[b] The ion abundance and S/N ratio values are from the average and standard deviations of 10 mass spectra acquired from different locations along the coffee ring (except for conventional MALDI). Each spectrum is the accumulation of 250 laser shots. The ion abundances trends reported here were consistent across multiple sample spots (≥ 5) and days.
[c] The signal enhancement factor is obtained by dividing the S/N ratio value of the coffee-ring enhanced measurement by the conventional MALDI-MS measurement.

The observed signal enhancement is primarily due to a peptide concentration effect in the ring itself, as the area covered by the ring is 15 to 30-fold less than the area covered by the entire sample spot. Consistent with this observation is the fact that peptide ion signals in the interior of the sample spot are always lower than peptide ion signals in the ring (Figure 3). There is no obvious correlation between signal enhancement values and how well-defined the coffee rings are, as NMs that form well-defined coffee rings (e.g. citrate NMs) often provide similar signal enhancements as NMs that do not form as well-defined coffee rings (e.g. Co-MXene). It should be noted, however, that while coffee ring formation is necessary for observing signal enhancement, it is not sufficient for signal enhancement, as GO forms a defined coffee ring (Figure S1h) but does not enhance peptide ion signal (Table 1).

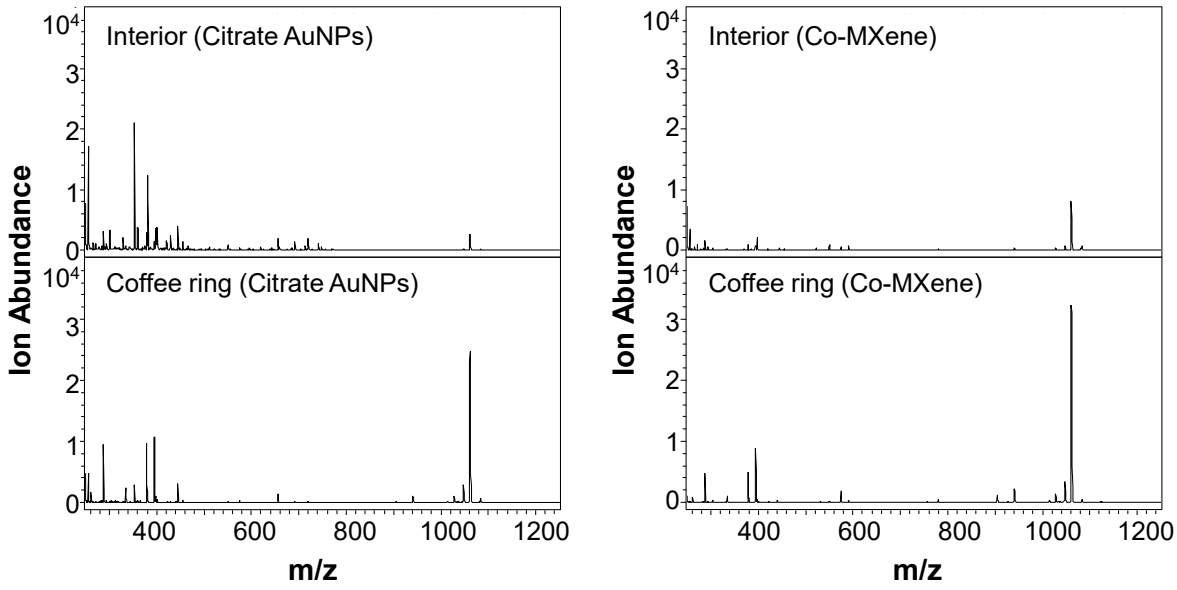

Figure 3: Representative MALDI mass spectra from a sample containing 0.125 mg/mL citrate AuNPs, 0.25 mg/mL of CHCA, and 1 μM of the peptide bradykinin (m/z 1060), showing the higher signal in the outer coffee ring (bottom) than in the interior of the sample spot (top).

NM-based signal enhancement changes in peptide mixtures

The effect of peptide identity on the coffee ring-induced signal enhancement was investigated for individual peptides and mixtures of peptides. Using a model set of seven peptides with a range of pI values, we observe signal enhancements relative to conventional MALDI for almost all the peptides when they are analyzed individually (Table 2, column two). We focus on only the TEGOH AuNPs, citrate AuNPs, GQD, and Co-MXene because these NMs provided the most consistently high peptide signal enhancements. The major exception to the signal enhancment trend is for the peptide ANP (SLRRSSCFGGR), which is not detected when GQDs are used. The reason for this behavior is unclear, but it is reproducible. Interestingly, this peptide can be detected at low levels in mixtures with the GQD. The specific factors that influence the magnitudes of the enhancement factors for each peptide and NM are not clear but will be investigated more fully in the future.

Table 2: Signal enhancement values relative to conventional MALDI matrix concentrations for peptides analyzed individually or in mixtures in coffee rings formed by the indicated NMs.

TEGOH (0.35 mg/mL)

Peptide	Individual	Mixture	Ratio	Peptide pI
1. Bradykinin	2.3	3.1	1.35	12.4
2. ANP	3.0	1.1	0.37	12.1
3. Kinetensin	1.3	2.3	1.77	11.1
4. Angiotensin I	3.0	1.5	0.50	7.91
5. Angiotensin II	5.9	1.3	0.22	7.76
6. Beta-amyloid	2.1	0.4	0.19	5.97
7. Preproenkephalin	0.8	--	0.00	3.37

Citrate AuNPs (0.125 mg/mL)

Peptide	Individual	Mixture	Ratio	Peptide pI
1. Bradykinin	3.0	4.0	1.33	12.4
2. ANP	3.9	1.1	0.28	12.1
3. Kinetensin	2.5	4.4	1.76	11.1
4. Angiotensin I	5.0	4.5	0.90	7.91
5. Angiotensin II	3.2	1.9	0.59	7.76
6. Beta-amyloid	7.3	3.8	0.52	5.97
7. Preproenkephalin	1.7	--	0.00	3.37

GQD (0.025 mg/mL)

Peptide	Individual	Mixture	Ratio	Peptide pI
1. Bradykinin	1.7	3.5	2.06	12.4
2. ANP	0.0	0.3	N.D.	12.1
3. Kinetensin	2.2	2.6	1.18	11.1
4. Angiotensin I	1.7	2.5	1.18	7.91
5. Angiotensin II	2.7	1.5	0.56	7.76
6. Beta-amyloid	1.4	1.3	0.92	5.97
7. Preproenkephalin	1.7	--	0.00	3.37

Co-MXene (0.25mg/mL)

Peptide	Individual	Mixture	Ratio	Peptide pI
1. Bradykinin	2.1	5.1	2.43	12.4
2. ANP	2.5	7.3	2.92	12.1
3. Kinetensin	2.4	7.6	3.17	11.1
4. Angiotensin I	1.5	0.9	0.60	7.91
5. Angiotensin II	4.1	1.8	0.44	7.76
6. Beta-amyloid	5.4	0.6	0.11	5.97
7. Preproenkephalin	1.9	--	0.00	3.37

An interesting observation is that the signal enhancement factors change substantially when the seven peptides are analyzed as a mixture (Table 2, column three). As a general trend, the signal enhancement factors for the peptides with high pI values either remain the same or increase, while the peptides with low pI values have decreased signal enhancement factors. The notable exception is for the peptide ANP when it is in a mixture with the two AuNPs. This peptide has a high pI value, but its signal enhancement decreases in the mixtures when TEGOH AuNPs or citrate AuNPs are used to form the coffee ring. We do not know the reason for this behavior, although we note that it is the only peptide with a Cys residue. Given the high affinity of thiol groups for AuNPs, it is possible that these strong interactions influence its signal when present in mixtures. Future work will investigate this possibility by examining other Cys-containing peptides.

We hypothesized that the signal enhancement changes in peptide mixtures might arise from competitive interactions between the peptides for limited binding sites on the NMs, allowing some peptides to be deposited with the NMs in the coffee ring while other peptides remain in the interior of the sample spot. To test this hypothesis, we performed two sets of experiments. First, the mixture of seven peptides and the individual NMs were allowed to form dried coffee rings, and then a small spot of 15 mg/mL of CHCA matrix was added to the interior of the dried sample spot, carefully avoiding the mixing of the higher CHCA concentration with the dry coffee ring (Figure 4). The purpose of this experiment was to see if there was some fractionation of peptides according to pI value when the initial coffee ring was formed. When the samples are analyzed in the ring versus the interior, we find that the high pI peptides have more abundant ion signals in the ring than in the interior, while the signal for the low pI peptides is about the same, as illustrated for citrate AuNPs (Figure 4).

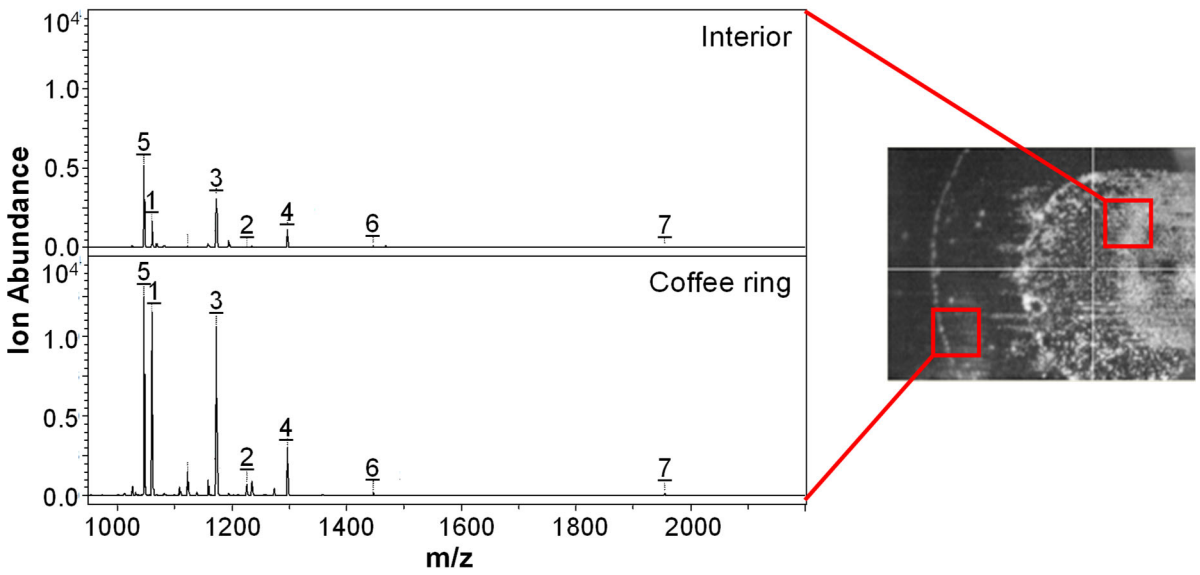

Figure 4: Representative MALDI mass spectra of the mixture of seven peptides shown in Table 2 after coffee ring formation with 0.125 mg/mL of citrate AuNPs and 0.25 mg/mL CHCA, followed the addition of 15 mg/mL of CHCA in the interior of the sample.

In a second set of experiments, we investigated the influence of NM concentration on the distribution of peptide signals. At low NM concentrations, the peptides are distributed more heterogeneously throughout the sample spot, as illustrated for 0.025 mg/mL concentrations of citrate AuNPs (Figure 5). Interestingly, the images for the higher pI peptides (e.g. RPPGFSPFR, IARRHPYFL) have more high intensity pixels (i.e. light colors) in the ring than the interior of the sample spot, while the low pI peptides (e.g. DRVYIHPF, YEVHHQKLVFF) tend to have fewer high intensity pixels in the ring. This observation is consistent with the high pI peptides having a higher signal enhancement when the mixtures are analyzed. When the NM concentrations are increased, as exemplified for 0.125 mg/mL citrate AuNPs (Figure 5), all the peptides become more homogeneously distributed in the coffee ring. These observations suggest that when enough NM interaction sites are present, more of the peptides are localized to the coffee ring. Together these two sets of data provide support for our hypothesis that the peptides compete for interactions sites

on the NMs, allowing some peptides to be selectively deposited on the outer ring especially at lower NM concentrations, while others remain more in the interior of the sample spot. In effect, the formation of the coffee ring by the NMs provides a crude fractionation of the peptides according to pI value. When one considers that the TEGOH AuNPs, citrate AuNPs, Co-MXene, and GQD all have negative zeta potentials (Table S1), it is probably not surprising that this crude fractionation favors the high pI peptides that are more positively charged.

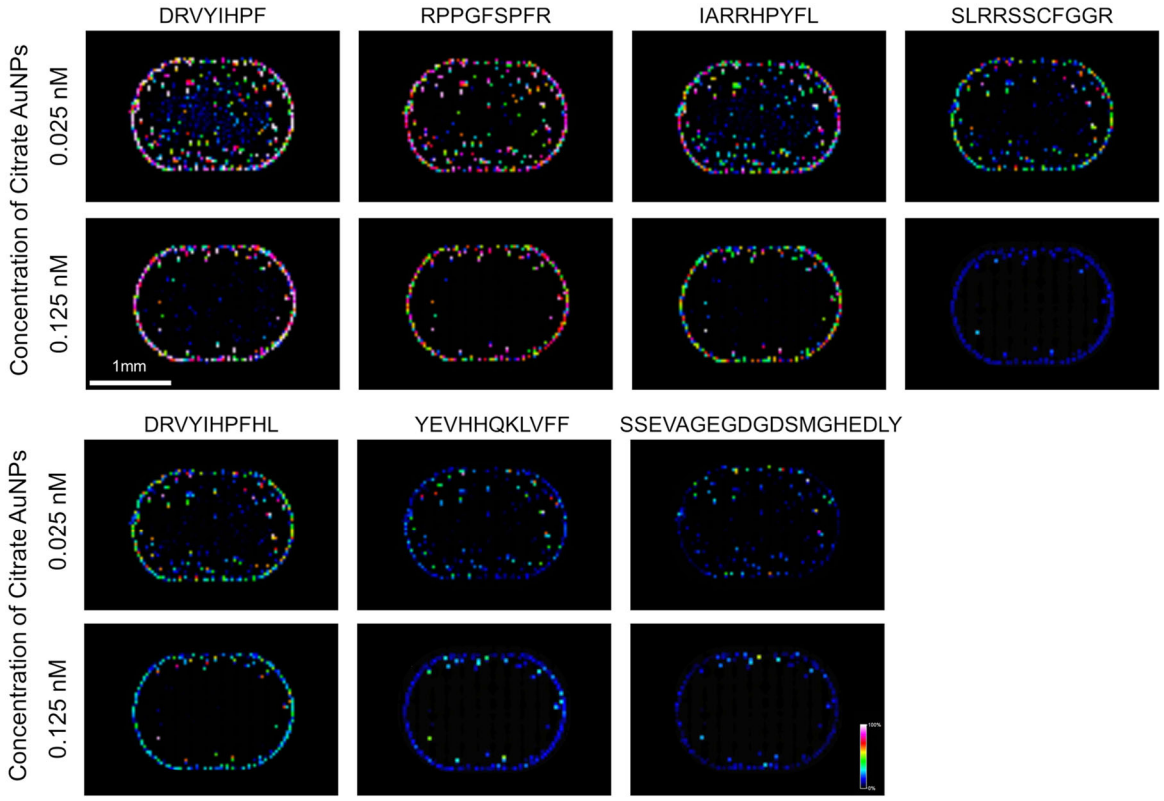

Figure 5: MALDI-MS images of peptides from the seven-peptide mixture after formation of coffee rings with two concentrations of citrate AuNPs (0.025 mg/mL and 0.125 mg/mL) and 0.25 mg/mL of CHCA.

To further illustrate the fractionation effect that occurs up coffee ring formation with the NMs, we analyzed a BSA digest. In its intact form, BSA is a ~66 kDa protein that has a pI value of about 4.7,[46] which means it has an excess of negatively-charged residues, such as Asp and Glu.

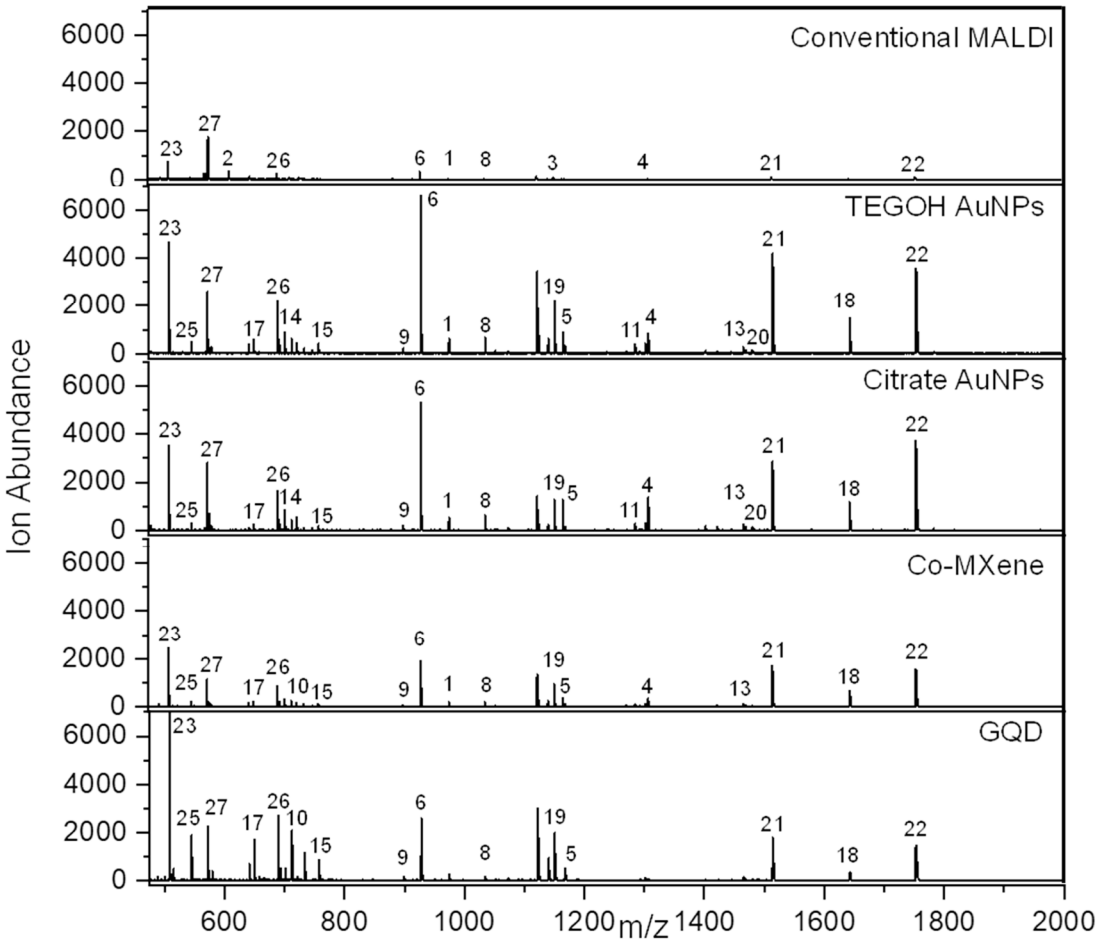

Figure 6: Representative MALDI mass spectra of a 1 µL sample of a 0.125 µM BSA digest by conventional MALDI (15 mg/mL CHCA) and from coffee-ring enhanced MALDI with different NMs, including 0.35 mg/mL TEGOH, 0.125 mg/mL citrate-AuNPs, 0.125 mg/mL Co-MXene, and 0.025 mg/mL GQD. In the NM preparations, the CHCA matrix concentration was 0.25 mg/mL. The numbers above each peak correspond to the detected peptides that are indicated in Table 3. The peptides that are indicated have a signal-to-noise ratio above 3 and were detected in at least 10 mass spectra.

Consequently, the vast majority of the peptides that are generated when it is digested have low pI values, although a few do have high pI values. During conventional MALDI-MS analysis with BSA concentrations (1 µL of a 0.125 µM solution) close to the detection limit of our MALDI-MS instrument, we find that relatively few peptides are detected, and they are a 50:50 mix of low pI (< 7) and high pI (> 7) peptides (Figure 6). When this same BSA digest concentration is analyzed after allowing it to form a coffee ring with various NMs, we find that the signal is much higher for

most peptides and several new peptides emerge due to the signal enhancement effect of the NMs. As can be seen in Table 3, about 90% of the newly detected peptides have pI values above 7. If we compare these results to the results from conventional MALDI at higher BSA concentrations (1 μL of a 0.5 μM solution), we measure four new peptides that were not detectable with conventional MALDI at the lower BSA concentrations, including the peptides RHPEYAVSVLLR (pI = 9.54), LGEYGFQNALIVR (pI = 6.81), ADLAKYICDNQDTISSK (pI = 4.01), and EC*C*HGDLLEC*ADDRADLAK (pI = 3.85). Of these four new peptides, only one of them has a pI value above 7 (i.e. RHPEYAVSVLLR). These results suggest that detection of the new peptides in the presence of the NMs is because of the more effective binding of higher pI peptides to the negatively-charged NMs, allowing them to be more effectively deposited on the coffee ring for enhanced detection.

Table 3: Peptides that are detected (as indicated by •) from a 1 μL sample of a 0.125 μM BSA digest by conventional MALDI or upon formation of coffee rings with the indicated nanomaterials.

Peptide[a]	m/z	pI[b]	Normal MALDI[c]	TEGOH[d]	Citrate AuNPs[e]	Co-MXene[f]	GQD[g]
1. DLGEEHFK	974	3.69	•	•	•	•	
2. AFDEK	609	3.93	•				
3. LVNELTEFAK	1164	4.15	•	•	•	•	
4. HLVDEPQNLIK	1306	5.17	•	•	•	•	
5. C*C*TKPESER	1167	6.14		•	•	•	•
6. YLYEIAR	928	6.56	•	•	•	•	•
7. LGEYGFQNALIVR	1480	6.81		•	•		
8. NEC*FLSHK	1034	7.04	•	•	•	•	•
9. LC*VLHEK	898	7.08		•	•	•	•
10. SEIAHR	712	7.55		•	•	•	•
11. HPEYAVSVLLR	1284	7.55		•	•	•	
12. DTHK	500	7.83					•
13. VGTRCCTKPESER	1465	8.10		•	•	•	
14. GACLLPK	701	8.84		•	•	•	•
15. GAC*LLPK	758	8.84		•	•	•	•
16. CASIQKFGER	1139	9.12		•	•	•	•
17. CASIQK	649	9.13		•	•	•	•

18. KVPQVSTPTLVEVSR	1640	9.90		•	•	•	•
19. LVTDLTKVHK	1154	9.93		•	•	•	
20. DTHKSEIAHRFK	1469	9.96		•	•		
21. QIKKQTALVELLK	1512	10.39	•	•	•	•	•
22. RHPEYAVSVLLRLAK	1752	10.39	•	•	•	•	•
23. HKPK	509	10.69	•	•	•	•	•
24. QIKK	516	10.69					•
25. VASLR	545	10.81		•	•	•	•
26. AWSVAR	689	10.90	•	•	•	•	•
27. QRLR	572	12.10	•	•	•	•	•

[a] Amino acid sequence of peptides that were detected with a signal-to-noise ratio above 3 in at least 10 mass spectra. Cysteines that are modified by iodoacetamide are indicated with an asterisk.
[b] Isoelectric point (pI) value estimated using the calculator at https://pepcalc.com/
[c] Conventional MALDI was performed using a CHCA concentration of 15 mg/mL.
[d] Coffee ring was formed with 0.35 mg/mL of TEGOH and 0.25 mg/mL of CHCA.
[e] Coffee ring was formed with 0.125 mg/mL of citrate AuNPs and 0.25 mg/mL of CHCA.
[f] Coffee ring was formed with 0.125 mg/mL of Co-MXene and 0.25 mg/mL of CHCA.
[g] Coffee ring was formed with 0.025 mg/mL of GQD and 0.25 mg/mL of CHCA.

Conclusions

The presence of NMs in solutions prepared for MALDI-MS analysis of peptides causes the formation of visible coffee rings as the samples dry. Peptides in solution are found to be enriched in these coffee rings, allowing for their signal to be enhanced up to 10-fold, as compared to conventional MALDI, when the laser is focused on the location of the rings. The identity of the nanomaterial itself has a modest effect on the observed signal enhancement, with smaller NMs tending to enhance signal somewhat more than larger NMs. Although, it should be noted that the formation of a coffee ring is necessary but not sufficient for signal enhancement, as GO NMs do not enhance peptide signals despite forming a well-defined coffee ring. When a mixture of peptides is combined with a given NM, the signal enhancements are found to depend on peptide charge, with positively-charged peptides being enhanced to a greater extent than negatively-charged peptides. This observation is most striking for a BSA digest, which contains an abundance of negatively-charged peptides, yet yields primarily positively-charged peptides upon ionization in the presence of NMs. We hypothesize that that the positively-charged peptides outcompete

negatively-charged peptides for binding sites on the negatively-charged NMs, allowing them to be preferentially enriched and detected in the coffee rings. Future work will seek to exploit this selective, enhanced detection by designing NM surfaces that can selectively binding different analytes.

Acknowledgments

Dr. Jutiporn Yukird would like to thank the Rachadapisek Sompote Fund at Chulalongkorn University for a postdoctoral fellowship. This work was also supported by the NSF grant CHE-1808199. We would like to thank Prof. Jiaqian Qin, Miss Dongdong Zhang, and Miss Benjawan Somchob for their advice in synthesizing the MXene derivatives and measuring their zeta potentials.

References

1. Beavis, R. C.; Chaudhary, T.; Chait, B. T., α-Cyano-4-hydroxycinnamic acid as a matrix for matrixassisted laser desorption mass spectromtry. *Org. Mass Spectrom.* **1992,** *27* (2), 156-158.
2. Zhu, X.; Papayannopoulos, I. A., Improvement in the detection of low concentration protein digests on a MALDI TOF/TOF workstation by reducing alpha-cyano-4-hydroxycinnamic acid adduct ions. *J. Biomol. Tech.* **2003,** *14* (4), 298-307.
3. Jaskolla, T. W.; Lehmann, W.-D.; Karas, M., 4-Chloro-α-cyanocinnamic acid is an advanced, rationally designed MALDI matrix. *Proc. Natl. Acad. Sci. USA* **2008,** *105* (34), 12200-12205.
4. Fournier, I.; Tabet, J. C.; Bolbach, G., Irradiation effects in MALDI and surface modifications: Part I: Sinapinic acid monocrystals. *Int. J. Mass Spectrom.* **2002,** *219* (3), 515-523.
5. Choi, H.; Lee, D.; Kim, Y.; Nguyen, H.-Q.; Han, S.; Kim, J., Effects of Matrices and Additives on Multiple Charge Formation of Proteins in MALDI–MS Analysis. *J. Am. Soc. Mass Spectrom.* **2019,** *30* (7), 1174-1178.

6. Salum, M. L.; Giudicessi, S. L.; Schmidt De León, T.; Camperi, S. A.; Erra-Balsells, R., Application of Z-sinapinic matrix in peptide MALDI-MS analysis. *J. Mass Spectrom.* **2017,** *52* (3), 182-186.

7. Kampmeier, J.; Dreisewerd, K.; Schürenberg, M.; Strupat, K., Investigations of 2,5-DHB and succinic acid as matrices for IR and UV MALDI. Part: I UV and IR laser ablation in the MALDI process. *Int. J. Mass Spectrom. Ion Processes* **1997,** *169-170*, 31-41.

8. Laštovičková, M.; Chmelik, J.; Bobalova, J., The combination of simple MALDI matrices for the improvement of intact glycoproteins and glycans analysis. *Int. J. Mass Spectrom.* **2009,** *281* (1), 82-88.

9. Calvano, C. D.; Monopoli, A.; Cataldi, T. R. I.; Palmisano, F., MALDI matrices for low molecular weight compounds: an endless story? *Anal. Bioanal. Chem.* **2018,** *410* (17), 4015-4038.

10. Rainer, M.; Qureshi, M. N.; Bonn, G. K., Matrix-free and material-enhanced laser desorption/ionization mass spectrometry for the analysis of low molecular weight compounds. *Anal. Bioanal. Chem.* **2011,** *400* (8), 2281-2288.

11. Shroff, R.; Muck, A.; Svatoš, A., Analysis of low molecular weight acids by negative mode matrix-assisted laser desorption/ionization time-of-flight mass spectrometry. *Rapid Commun. Mass Spectrom.* **2007,** *21* (20), 3295-3300.

12. Leopold, J.; Popkova, Y.; Engel, K. M.; Schiller, J., Recent Developments of Useful MALDI Matrices for the Mass Spectrometric Characterization of Lipids. *Biomolecules* **2018,** *8* (4), 173.

13. Shi, C. Y.; Deng, C. H., Recent advances in inorganic materials for LDI-MS analysis of small molecules. *Analyst* **2016,** *141* (10), 2816-2826.

14. Wang, J.; Liu, Q.; Liang, Y.; Jiang, G., Recent progress in application of carbon nanomaterials in laser desorption/ionization mass spectrometry. *Anal. Bioanal. Chem.* **2016,** *408* (11), 2861-2873.

15. Arakawa, R.; Kawasaki, H., Functionalized Nanoparticles and Nanostructured Surfaces for Surface-Assisted Laser Desorption/Ionization Mass Spectrometry. *Anal. Sci.* **2010,** *26* (12), 1229-1240.

16. Yagnik, G. B.; Hansen, R. L.; Korte, A. R.; Reichert, M. D.; Vela, J.; Lee, Y. J., Large Scale Nanoparticle Screening for Small Molecule Analysis in Laser Desorption Ionization Mass Spectrometry. *Anal. Chem.* **2016,** *88* (18), 8926-8930.

17. Xu, S.; Li, Y.; Zou, H.; Qiu, J.; Guo, Z.; Guo, B., Carbon Nanotubes as Assisted Matrix for Laser Desorption/Ionization Time-of-Flight Mass Spectrometry. *Anal. Chem.* **2003,** *75* (22), 6191-6195.

18. Marsico, A. L. M.; Creran, B.; Duncan, B.; Elci, S. G.; Jiang, Y.; Onasch, T. B.; Wormhoudt, J.; Rotello, V. M.; Vachet, R. W., Inkjet-Printed Gold Nanoparticle Surfaces for the Detection of Low Molecular Weight Biomolecules by Laser Desorption/Ionization Mass Spectrometry. *J. Am. Soc. Mass Spectrom.* **2015,** *26* (11), 1931-1937.

19. Lei, C.; Qian, K.; Noonan, O.; Nouwens, A.; Yu, C., Applications of nanomaterials in mass spectrometry analysis. *Nanoscale* **2013,** *5* (24), 12033-12042.

20. Scida, K.; Stege, P. W.; Haby, G.; Messina, G. A.; García, C. D., Recent applications of carbon-based nanomaterials in analytical chemistry: Critical review. *Anal. Chim. Acta* **2011,** *691* (1), 6-17.

21. Shiea, J.; Huang, J.-P.; Teng, C.-F.; Jeng, J.; Wang, L. Y.; Chiang, L. Y., Use of a Water-Soluble Fullerene Derivative as Precipitating Reagent and Matrix-Assisted Laser Desorption/Ionization Matrix To Selectively Detect Charged Species in Aqueous Solutions. *Anal. Chem.* **2003,** *75* (14), 3587-3595.

22. Zhou, L.; Deng, H.; Deng, Q.; Zheng, L.; Cao, Y., Analysis of three different types of fullerene derivatives by laser desorption/ionization time-of-flight mass spectrometry with new matrices. *Rapid Commun. Mass Spectrom.* **2005,** *19* (23), 3523-3530.

23. Hong, S. H.; Kim, J. I.; Kang, H.; Yoon, S.; Kim, D. E.; Jung, W.; Yeo, W. S., Detection and quantification of the Bcr/Abl chimeric protein on biochips using LDI-TOF MS. *Chem. Commun.* **2014,** *50* (37), 4831-4.

24. Kim, Y. K.; Min, D. H., Preparation of the hybrid film of poly(allylamine hydrochloride)-functionalized graphene oxide and gold nanoparticle and its application for laser-induced desorption/ionization of small molecules. *Langmuir* **2012,** *28* (9), 4453-8.

25. McLean, J. A.; Stumpo, K. A.; Russell, D. H., Size-Selected (2−10 nm) Gold Nanoparticles for Matrix Assisted Laser Desorption Ionization of Peptides. *J. Am. Chem. Soc.* **2005,** *127* (15), 5304-5305.

26. Pilolli, R.; Palmisano, F.; Cioffi, N., Gold nanomaterials as a new tool for bioanalytical applications of laser desorption ionization mass spectrometry. *Anal. Bioanal. Chem.* **2012,** *402* (2), 601-623.

27. Castellana, E. T.; Russell, D. H., Tailoring Nanoparticle Surface Chemistry to Enhance Laser Desorption Ionization of Peptides and Proteins. *Nano Lett.* **2007,** *7* (10), 3023-3025.

28. Chen, C.-T.; Chen, Y.-C., Fe_3O_4/TiO_2 Core/Shell Nanoparticles as Affinity Probes for the Analysis of Phosphopeptides Using TiO_2 Surface-Assisted Laser Desorption/Ionization Mass Spectrometry. *Anal. Chem.* **2005,** *77* (18), 5912-5919.

29. Kim, J. I.; Park, J. M.; Hwang, S. J.; Kang, M. J.; Pyun, J. C., Top-down synthesized TiO_2 nanowires as a solid matrix for surface-assisted laser desorption/ionization time-of-flight (SALDI-TOF) mass spectrometry. *Anal. Chim. Acta.* **2014,** *836*, 53-60.

30. Lee, K. H.; Chiang, C. K.; Lin, Z. H.; Chang, H. T., Determining enediol compounds in tea using surface-assisted laser desorption/ionization mass spectrometry with titanium dioxide nanoparticle matrices. *Rapid Commun. Mass Spectrom.* **2007,** *21* (13), 2023-30.

31. Wu, Q.; Chu, J. L.; Rubakhin, S. S.; Gillette, M. U.; Sweedler, J. V., Dopamine-modified TiO_2 monolith-assisted LDI MS imaging for simultaneous localization of small metabolites and lipids in mouse brain tissue with enhanced detection selectivity and sensitivity. *Chem. Sci.* **2017,** *8* (5), 3926-3938.

32. Hu, J.-B.; Chen, Y.-C.; Urban, P. L., Coffee-ring effects in laser desorption/ionization mass spectrometry. *Anal. Chim. Acta* **2013,** *766*, 77-82.

33. Kim, M.-J.; Park, J.-M.; Noh, J.-Y.; Yun, T. G.; Kang, M.-J.; Ku, N. S.; Lee, E. H.; Park, K. H.; Park, M. S.; Lee, S.-G.; Pyun, J.-C., Coffee Ring Effect Free TiO2 Nanotube Array for Quantitative Laser Desorption/Ionization Mass Spectrometry. *ACS Appl. Nano Mater.* **2020,** *3* (9), 9249-9259.

34. Wen, X.; Dagan, S.; Wysocki, V. H., Small-Molecule Analysis with Silicon-Nanoparticle-Assisted Laser Desorption/Ionization Mass Spectrometry. *Anal. Chem.* **2007,** *79* (2), 434-444.

35. Kawasaki, H.; Sugitani, T.; Watanabe, T.; Yonezawa, T.; Moriwaki, H.; Arakawa, R., Layer-by-Layer Self-Assembled Mutilayer Films of Gold Nanoparticles for Surface-Assisted Laser Desorption/Ionization Mass Spectrometry. *Anal. Chem.* **2008,** *80* (19), 7524-7533.

36. Kim, Y.-K.; Wang, L.-S.; Landis, R.; Kim, C. S.; Vachet, R. W.; Rotello, V. M., A layer-by-layer assembled MoS2 thin film as an efficient platform for laser desorption/ionization mass spectrometry analysis of small molecules. *Nanoscale* **2017,** *9* (30), 10854-10860.

37. Wu, H.-P.; Yu, C.-J.; Lin, C.-Y.; Lin, Y.-H.; Tseng, W.-L., Gold nanoparticles as assisted matrices for the detection of biomolecules in a high-salt solution through laser desorption/ionization mass spectrometry. *J. Am. Soc. Mass Spectrom.* **2009,** *20* (5), 875-882.

38. Wu, H.-P.; Su, C.-L.; Chang, H.-C.; Tseng, W.-L., Sample-First Preparation: A Method for Surface-Assisted Laser Desorption/Ionization Time-of-Flight Mass Spectrometry Analysis of Cyclic Oligosaccharides. *Anal. Chem.* **2007,** *79* (16), 6215-6221.

39. Marsico, A. L. M.; Duncan, B.; Landis, R. F.; Tonga, G. Y.; Rotello, V. M.; Vachet, R. W., Enhanced Laser Desorption/Ionization Mass Spectrometric Detection of Biomolecules Using Gold Nanoparticles, Matrix, and the Coffee Ring Effect. *Anal. Chem.* **2017,** *89* (5), 3009-3014.

40. Mampallil, D.; Eral, H. B., A review on suppression and utilization of the coffee-ring effect. *Adv.Colloid Interf. Sci.* **2018,** *252*, 38-54.

41. Lohani, D.; Basavaraj, M. G.; Satapathy, D. K.; Sarkar, S., Coupled effect of concentration, particle size and substrate morphology on the formation of coffee rings. *Colloids Surf. A Physicochem. Eng. Asp.* **2020,** *589*, 124387.

42. Zang, D.; Tarafdar, S.; Tarasevich, Y. Y.; Dutta Choudhury, M.; Dutta, T., Evaporation of a Droplet: From physics to applications. *Physics Rep.* **2019,** *804*, 1-56.

43. Neampet, S.; Ruecha, N.; Qin, J.; Wonsawat, W.; Chailapakul, O.; Rodthongkum, N., A nanocomposite prepared from platinum particles, polyaniline and a Ti3C2 MXene for amperometric sensing of hydrogen peroxide and lactate. *Microchimica Acta* **2019,** *186* (12), 752.

44. Chon, C. H.; Paik, S.; Tipton, J. B.; Kihm, K. D., Effect of Nanoparticle Sizes and Number Densities on the Evaporation and Dryout Characteristics for Strongly Pinned Nanofluid Droplets. *Langmuir* **2007,** *23* (6), 2953-2960.

45. Bansal, L.; Seth, P.; Murugappan, B.; Basu, S., Suppression of coffee ring: (Particle) size matters. *Appl. Phys. Lett.* **2018,** *112*, 211605.

46. Li, R.; Wu, Z.; Wangb, Y.; Ding, L.; Wang, Y., Role of pH-induced structural change in protein aggregation in foam fractionation of bovine serum albumin. *Biotechnol. Rep.* **2016,** *9*, 46-52.

For Table of Contents Use Only

Enhanced and Selective MALDI-MS Detection of Peptides via the Nanomaterial-Dependent Coffee Ring Effect

Jutiporn Yukird, Cameron J. Kaminsky, Orawon Chailapakul, Nadnudda Rodthongkum,* and Richard W. Vachet*

A variety of different nanomaterials can form coffee rings upon drying from liquid samples that contain low concentrations of a MALDI matrix and peptides. Upon laser irradiation of these coffee rings, peptide ion signals can be enhanced compared to conventional MALDI-MS, and peptide detection selectivity can be achieved based on the nanomaterial surface properties.